



Selective localization of multi-walled carbon nanotubes in thermoplastic elastomer blends: An effective method for tunable resistivity–strain sensing behavior



Mizhi Ji, Hua Deng*, Dongxue Yan, Xiaoyu Li, Lingyan Duan, Qiang Fu*

College of Polymer Science and Engineering, State Key Laboratory of Polymer Materials Engineering, Sichuan University, Chengdu 610065, PR China

ARTICLE INFO

Article history:

Received 8 August 2013

Received in revised form 6 November 2013

Accepted 15 November 2013

Available online 1 December 2013

Keywords:

A. Polymer–matrix composites (PMCs)

B. Electrical properties

C. Deformation

C. Modelling

ABSTRACT

Conductive network morphology and interfacial interaction play important roles in determining resistivity–strain (ρ – ε) sensing behavior of conductive polymer composites (CPCs). In this work, thermoplastic elastomer blends consisting of poly(styrene–butadiene–styrene) block polymer (SBS) and thermoplastic polyurethane (TPU) were fabricated via different melt processing procedures, which could tune the above two issues simultaneously by selectively localizing multi-walled carbon nanotubes (MWCNTs) in SBS, TPU and both in SBS and TPU, respectively. It is observed that the composite fibers with selectively localized MWCNTs show distinct different ρ – ε sensing behavior. Work of adhesion calculation suggests stronger interfacial interaction between MWCNTs and SBS, however, wetting coefficient calculation indicates slightly better wetting of MWCNTs with TPU. Because of such stronger interaction and poorer dispersion, the composite fiber with MWCNTs distributed in SBS exhibits higher ρ – ε sensitivity than its counterpart with MWCNTs distributed in TPU, and with MWCNTs distributed in both phases, the ρ – ε sensitivity lies in between. Moreover, the ρ – ε sensing behavior was fitted with a model based on tunneling theory by Simmons. It is suggested that the change in tunneling distance and the number of conductive pathways could be accelerated significantly under strong interfacial interaction. This study could offer a new pathway and provide a guideline for the preparation of high-performance CPC resistivity–strain sensors with tunable sensitivity.

© 2013 Elsevier Ltd. All rights reserved.

1. Introduction

Conductive polymer composites (CPCs) have been an active research topic for several decades due to their wide range of applications and ease of processing [1]. In recent years, CPCs have been extensively investigated as sensors to detect various external stimuli, such as strain [2,3], damage [4,5], temperature [6,7], liquids [8–10], vapors [11–13] and PH [14]. In terms of resistivity–strain sensors, CPCs are considered as promising candidates to detect resistivity change induced by strain. The practical use of carbon nanotube (CNT) structure demonstrates their application in the field of sensing technology as an active part of sensing structural composites [15,16]. Thermoplastic elastomer (TPE) with combined characteristics of rubber and plastic, has gained considerable amount of attention recently, which is critically important for the application of a good engineering thermoplastic material. Thus, CPCs containing TPE and CNT are valued as the prospective stretchable resistivity–strain sensors for detecting dangerous

deformations and vibrations of mechanical parts in many fields of science and engineering.

A tunable resistivity–strain dependency (resistivity–strain sensitivity) is often required for different applications. Thus, the control of sensitivity is one of the most important issues for the preparation of resistivity–strain sensors. To modify the resistivity–strain sensitivities of these sensors, several methods have been proposed. Recently, our group has reported that mixed fillers containing CNTs and metallic particles in different volume ratios can be used to modify the resistivity–strain sensitivity of CPC fibers [17]. Dang et al. observed that CNTs with higher aspect ratio are preferred for higher sensitivity to pressure in CNT/silicone rubber composites [18]. Murugaraj et al. demonstrated that narrow distribution of tunnel gaps between overlapping nanochannels is responsible for the high electromechanical sensitivity of their CPCs [19]. And Hwang et al. reported that the concentration of poly(3-hexylthiophene) (P3HT) plays an important role in the piezoresistive sensitivity of P3HT-wrapped CNT/poly(dimethylsiloxane) composites [20].

In above investigations, different strategies have been considered for controlling resistivity–strain sensitivity in CPCs, however, they exhibit relative narrow range of tunable sensitivity.

* Corresponding authors. Tel.: +86 28 8546 0953 (H. Deng). Tel./fax: +86 28 8546 1795 (Q. Fu).

E-mail addresses: huadeng@scu.edu.cn (H. Deng), qiangfu@scu.edu.cn (Q. Fu).

Systematic and efficient methods are still necessary for modifying sensitivity. Therefore, fundamental aspects of resistivity–strain sensing CPCs need to be reconsidered for the preparation of high performance sensors with tunable sensitivity. In CPCs, conductive networks are formed with conductive fillers in insulating polymer matrixes, which provide continuous conductive pathways for electrical current. In the case of entangled conductive networks, the response of electrical property to strain is governed by both conductive network morphology and interfacial interaction between filler and polymer matrix. As a result, these two issues should be regarded as the key factors in modifying resistivity–strain sensitivity. Nevertheless, these issues have barely been investigated simultaneously [21].

Polymer blending has been extensively studied as one of the most important methods to modify conductive network structure in CPCs [22–24]. As polymer blends offer more interface and phase structures in CPCs, different conductive network morphologies can be constructed from selective localization of conductive fillers in different phases, not to mention the abundant change of phase morphology in polymer blends during stretching [25]. Furthermore, different polymers tend to have different interfacial interactions with fillers due to their difference in chemical nature. Thus, using polymer blends can be considered as an effective method to tune both conductive network morphology and interfacial interaction in CPCs for the control of resistivity–strain sensitivity. However, such a method has yet to be reported for CPCs based on resistivity–strain sensors.

Herein, we utilize polymer blends consisting of poly(styrene–butadiene–styrene) block polymer (SBS) and thermoplastic polyurethane (TPU) to fabricate CPC resistivity–strain sensors. Efforts are carried out to selectively distribute conductive fillers in one or two of the polymer phases. The effect of conductive filler location in polymer blends on the resistivity–strain sensing properties is systematically investigated. The conductive network morphology before and after stretching; the orientation of polymer matrix and conductive filler under strain is also studied to investigate the electrical property–strain sensing behavior of these CPCs. Finally, an analytical model is used to further understand the change of electrical property under strain.

2. Experimental

2.1. Materials

Multi-walled carbon nanotubes (MWCNTs, Nanocyl 7000, Nanocyl S.A.) were used as conductive fillers in the composites. According to producer, these MWCNTs have an average diameter of 10 nm, length of 1.5 μm and a specific surface area of 250–300 m^2/g . SBS with S/B ratio of 40/60 and trademark of SBS-792 was kindly provided by Baling Company of Sinopec Co. Ltd., China. Polyester based TPU (IROGRAN 455-200) was provided by Huntsman Company.

2.2. Sample preparation

MWCNT composites were prepared in a Hakke internal mixer. All blends were mixed at 60 rpm under 160 °C. SBS/TPU/MWCNT composites were melt-blended via applying three different procedures: blending of premixed SBS-MWCNT or TPU-MWCNT composites with the respective unfilled polymer in a second step, direct blending of SBS-MWCNT and TPU-MWCNT in a second step. In order to minimize the possible transition of MWCNTs during the second step, these precompounds were melted in the mixer for 10 min while the mixing time of the second step was 5 min. Then, these composites were extruded as fibers with piston-mode

Rosand RH70 (Malvern, Bohlin Instruments) capillary rheometer. The experimental procedures are summarized in Fig. 1.

In this paper, samples were denoted as $A-x\text{NT}/B$, where A and B represent the elastomer matrixes, x represents MWCNT content in A phase. $A-x\text{NT}/B$ also represents that MWCNTs were premixed in A phase at first. For example, SBS-8NT/TPU represents that SBS-MWCNT containing 8 wt.% of MWCNTs was mixed with TPU in a second step.

2.3. Characterization

Contact angles were measured in a sessile drop mould with KRUSS DSA100. Pure elastomer samples for contact angle measurements were compression moulded at 180 °C under 10 MPa pressure for 10 min then cooled to 20 °C. Contact angles were measured on 3 ml of wetting solvent at 20 °C, and the results reported were the mean values of 3 replicates. The surface tensions, dispersion and polar components of these elastomers can be also obtained from contact angle measurements.

With gauge length of 50 mm, the melt-spun fibers were clamped between a pair of alumina electrodes in a SANS CMT4000 universal test machine. Electrical resistance was measured with a Keithley 6487 picoammeter under a constant voltage of 1 V to avoid strong electrical current within the sample. Both the resistance measurement set-up and tensile test machine were interfaced with a computer to record the resistance change during stretching. A constant rate of 10 mm/min was used for the simultaneous resistance–strain measurement. Cyclic stretching and recovery was also conducted to investigate the dynamic resistivity–strain behavior. It should be noted that the sample with a resistivity above 10^4 is considered as non-conductive due to the limitation of current set-up.

Morphological studies were carried out using a scanning electron microscope (SEM, JEOL JSM-5900LV) under an accelerating voltage of 20 kV. To investigate the conductive networks below the sample surface, un-coated specimens were used. The conductive networks in the polymer matrix are charged to emit enriched secondary electrons to make them visible [26]. In addition, these fiber specimens were cryogenically fractured in a direction perpendicular to flow direction in liquid nitrogen and the fracture surfaces were coated with a thin layer of gold to examine the blend morphology and MWCNT dispersion in the composites.

Polarized Raman spectra was recorded on a micro-Raman spectrometer (JY HR800) equipped with a microscope. Excitation was provided by He–Ne at 786 nm. A beam size of 1 μm was used. In order to determine the orientation level of MWCNTs, the dichroism Raman spectra were achieved by recording Raman spectroscopy along two directions normal between each other, which were parallel and perpendicular to the long-axis (length) direction of fiber, respectively. All spectra were baseline corrected and the peak position and intensity were fitted in the range from 1000 cm^{-1} to 2000 cm^{-1} .

3. Results and discussion

3.1. Resistivity–strain sensing behavior of SBS/TPU/MWCNT composite fibers

The resistivity–strain sensing behavior is examined by measuring the electrical resistance as a function of uniaxial strain to evaluate the potential of these fibers as resistivity–strain sensors. Fig. 2(a) shows the resistivity–strain dependence of SBS/TPU/MWCNT composite fibers. In spite of different starting points, all samples demonstrate a definitive trend where the resistivity increases logarithmically with increasing strain. As indicated by the slope coefficient of resistivity–strain (ρ – ϵ) curve, SBS-4NT/

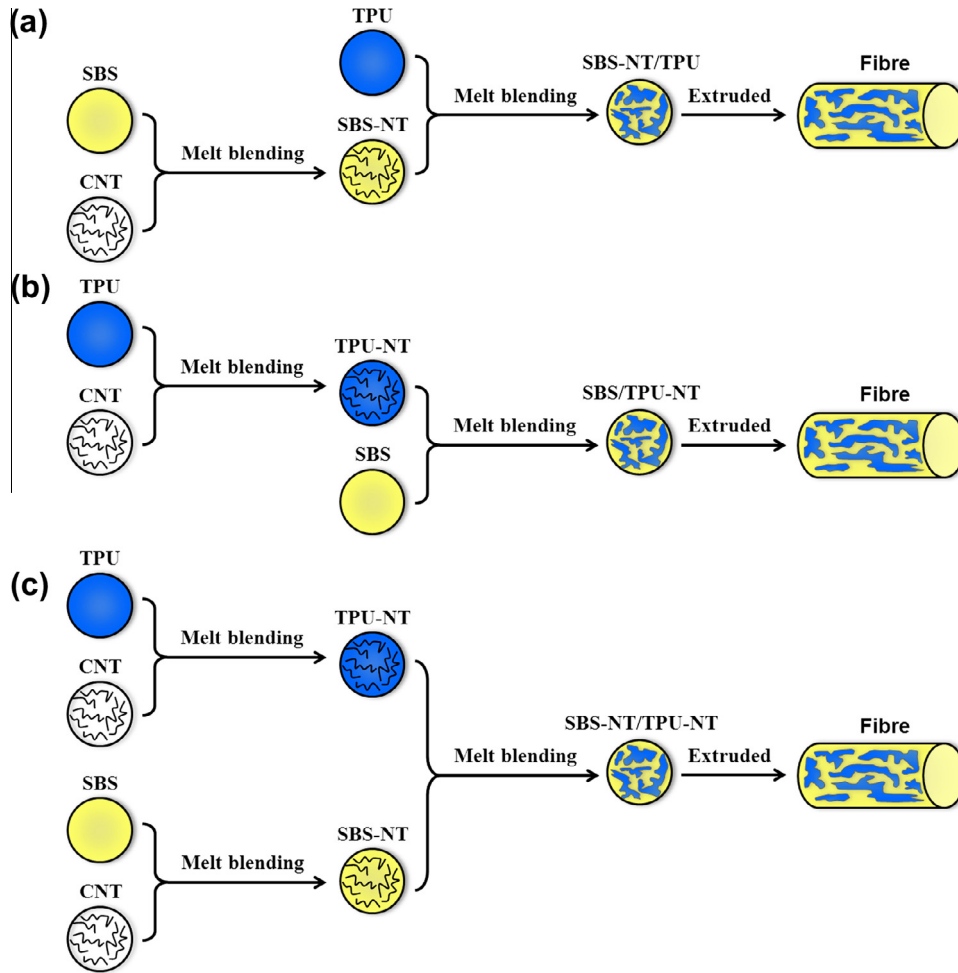


Fig. 1. Sketch of the processing procedures: (a) SBS-NT/TPU, (b) SBS/TPU-NT and (c) SBS-NT/TPU-NT composite fibers.

TPU-4NT exhibits higher ρ - ε sensitivity than SBS/TPU-8NT while SBS-8NT/TPU possesses the highest ρ - ε sensitivity. The different ρ - ε sensitivities of these composite fibers should be attributed to the selective localization of MWCNTs in these blends, which will be further explained in the following Sections 3.2 and 3.3. As shown in Fig. 2(a), for strains below 80%, it is observed that the ρ - ε sensitivity does not vary with different filler distributions. This behavior might be attributed to the fact that these conductive networks are very dense under such small strains and only deform slightly during stretching. For strains above 80%, the conductive networks in the composite fibers deform significantly during stretching and selective localization of MWCNTs in thermoplastic elastomer blends becomes the main factor resulting in different ρ - ε sensitivities of SBS-8NT/TPU and SBS/TPU-8NT. Similar result has been reported in our previous study for TPU based CPCs containing MWCNTs and metallic particles as conductive filler [17]. Nevertheless, it can be noticed that inflection points of the ρ - ε curves for SBS-8NT/TPU and SBS/TPU-8NT are different from each other. In this work, we have investigated the effect of selective localization of MWCNTs in thermoplastic elastomer blends on the tunable ρ - ε sensing behavior of CPCs. The phenomenon of different inflection points will be further investigated in our ongoing work.

As strain-sensing application often requires reversible strain loadings, composite fibers were subjected to strain-sensing tests using a cyclic loading profile with 80% minimum strain and 120% maximum strain. Fig. 2(b) shows the relative resistance (R/R_0)

change of these composite fibers during cyclic stretching. For SBS-8NT/TPU, it is observed that the resistivity changes simultaneously with applied strain, which generally increases with increasing strain and decreases with decreasing strain. For SBS-4NT/TPU-4NT and SBS/TPU-8NT, the sensing signals are not monotone with shoulder peaks observed during these cycles, showing almost an inverse relationship between resistivity and strain [15,27]. This phenomenon might originate from the competition between destruction and reconstruction of conductive pathways during dynamic loadings [28]. In analogy with the result in Fig. 2(a), SBS-8NT/TPU presents the highest ρ - ε sensitivity, giving the strongest signal during the cyclic stretching. Furthermore, a gradual decrease in resistivity peaks is observed in the first few cycles, which is thought to be caused by the formation of additional conductive pathways through a breakdown of the interface between polymer and fillers [29].

To further understand ρ - ε sensing behavior of blends based CPCs, different elastomers with the same content of MWCNTs were studied. The resistivity change of TPE-MWCNT composite fibers with 4 wt.% MWCNTs versus strain was plotted as shown in Fig. 2(c and d) and the resistivity increases exponentially with increasing strain. It can be observed that the two samples show different ρ - ε sensing behaviors. The resistivity of SBS-4NT increases rapidly with increasing strain, indicating much higher ρ - ε sensitivity for SBS-4NT in comparison with TPU-4NT. By comparing Fig. 2(a) with (c), it can be noted that the selective localization of the same amount of MWCNTs (overall 4 wt.%) has important

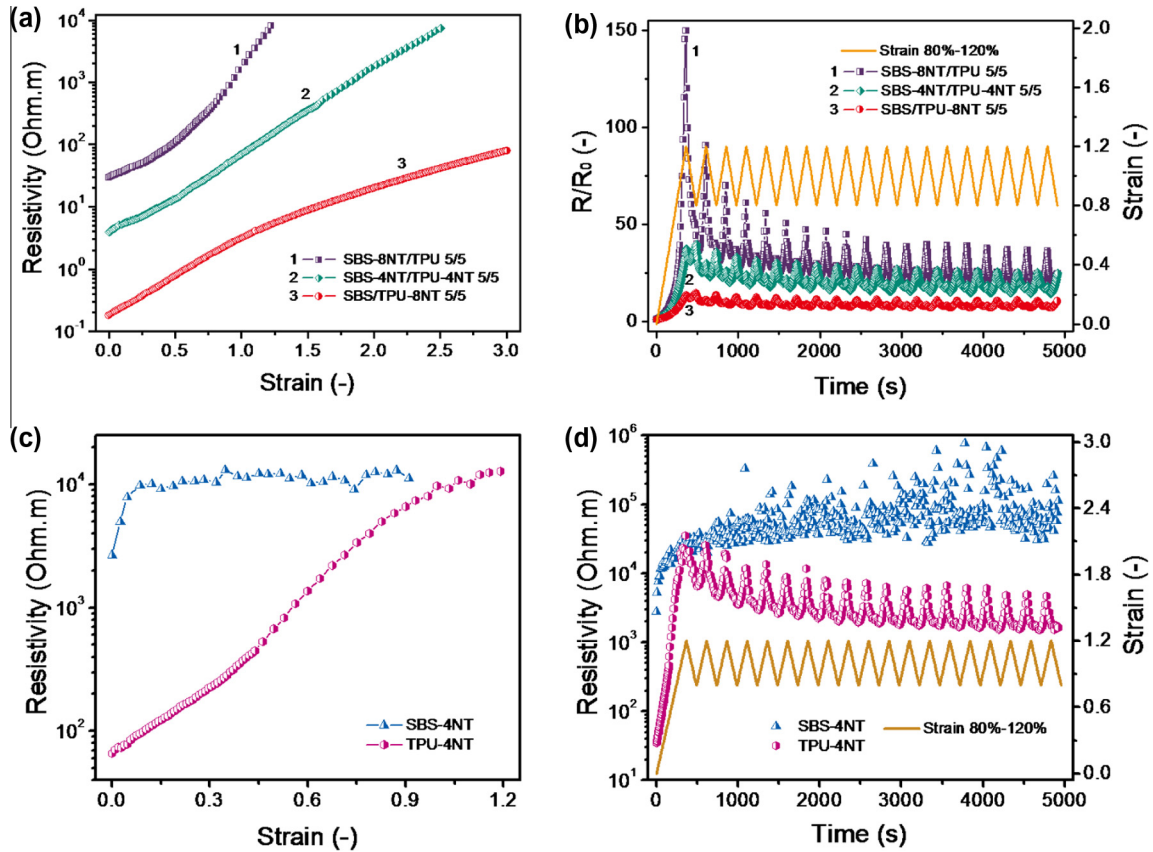


Fig. 2. Resistivity–strain sensing behavior: (a) resistivity versus strain and (b) normalized resistivity versus time relationship of SBS/TPU/MWCNT composite fibers; (c) resistivity versus strain and (d) resistivity versus time relationship of SBS-4NT and TPU-4NT composite fibers.

Table 1

Surface tensions of MWCNT, SBS and TPU at 20 °C.

Materials	Surface tensions (mN/m)		
	Total (γ)	Dispersive part (γ^d)	Polar part (γ^p)
MWCNT ^a	27.8	17.6	10.2
SBS	48.8	36.2	12.6
TPU	41.7	30.4	11.3

^a According to Barber et al. [48].

Table 2

Interfacial energies and wetting coefficients as calculated using harmonic and geometric mean equations.

Calculation methods	Interfacial energies (mN/m)			Wetting coefficient (ω_a mN/m)
	$\gamma_{\text{SBS-CNT}}$	$\gamma_{\text{TPU-CNT}}$	$\gamma_{\text{SBS-TPU}}$	
According to harmonic mean equation	6.68	3.45	0.58	5.56
According to geometric mean equation	3.44	1.76	0.29	5.79

influence on the electrical property as well as ρ - ϵ sensitivity of these CPCs. The underlying mechanism is thought to be closely related with the differences in conductive network morphology and interfacial interaction caused by selective localization of MWCNTs in the blends. Following study (Sections 3.2 and 3.3) is carried out to investigate these issues.

3.2. Morphology of initial conductive networks: selective localization of MWCNTs in the blends

In CPCs based on polymer blends, the conductive fillers may be located unevenly between polymer phases. The resulting electrical properties are influenced by the localization of conductive fillers as well as blend morphology [30,31]. As well known, the selective localization of CNTs in polymer blends is commonly explained by the concept of wetting coefficient [32–39]. In equilibrium state, the localization of CNTs in polymer blends can be predicted by the minimization of interfacial energy. According to Young's equation, it is possible to find the equilibrium position of CNTs by evaluating the wetting coefficient ω_a , as defined in Eq. (1) [40]:

$$\omega_a = \frac{\gamma_{\text{SBS-CNT}} - \gamma_{\text{TPU-CNT}}}{\gamma_{\text{SBS-TPU}}} \quad (1)$$

In this equation, γ is the different interfacial energies of polymer–filler in the numerator and that of polymer–polymer in the denominator. The wetting coefficient is most commonly interpreted in a way that, for value < -1 , the fillers are predicted to be located in the polymer phase named first (here SBS), and for value > 1 , in the polymer phase named second (here TPU). In the interval of ω_a value between -1 and 1 , the fillers are predicted to be located at the interface.

The interfacial energies (see Table 2) can be evaluated from the surface tensions of the components (see Table 1), using both the harmonic-mean and the geometric-mean equations [40]. The harmonic-mean equation (Eq. (2)) is valid between low-energy materials and the geometric-mean equation (Eq. (3)) is valid between a low-energy material and a high-energy material:

$$\gamma_{12} = \gamma_1 + \gamma_2 - 4 \left(\frac{\gamma_1^d \gamma_2^d}{\gamma_1^d + \gamma_2^d} + \frac{\gamma_1^p \gamma_2^p}{\gamma_1^p + \gamma_2^p} \right) \quad (2)$$

$$\gamma_{12} = \gamma_1 + \gamma_2 - 2 \left(\sqrt{\gamma_1^d \gamma_2^d} + \sqrt{\gamma_1^p \gamma_2^p} \right) \quad (3)$$

where γ_1, γ_2 are the surface tensions of components 1, 2; γ_1^d, γ_2^d are the dispersive parts of the surface tensions of components 1, 2; and γ_1^p, γ_2^p are the polar parts of the surface tensions of components 1, 2.

For these two methods, the calculated wetting coefficients are positive (and even above 1, see Table 2), as the interfacial energy between TPU and MWCNT ($\gamma_{\text{TPU-CNT}}$) is slightly lower than that between SBS and MWCNT ($\gamma_{\text{SBS-CNT}}$), which indicates a slightly better wetting of MWCNT with TPU. Therefore, the TPU–MWCNT pair tends to be formed to minimize the total free energy in the ternary composite of SBS/TPU/MWCNT. However, besides thermodynamic driving forces, the selective localization of CNTs in polymer blends is also related with kinetic factors [41,42], such as blending procedures, blending time, and shear strength. The final localization behavior of CNTs in polymer blends is mainly determined by the interplay between thermodynamic driving forces and kinetic factors.

Thus, in highly compatible SBS/TPU/MWCNT blends with only small differences in surface energy and polarity of blend compositions, the selective localization of MWCNTs only in one phase can be simply achieved via different melt blending procedures as shown in Fig. 1. The three different mixing procedures are all two-step blending, in which the mixing time of the second step (5 min) is much shorter than that of premixing step (10 min) to

minimize the possible transition of MWCNTs during the second step.

In the case of SBS/TPU/MWCNT blends, high compatibility between SBS and TPU is observed in Fig. 3 as evidenced by the unobvious interface. The transformations of dispersed phase and continuous phase with the change of phase ratios (3/7, 5/5, 7/3) can be easily observed in each blend, which reveals the morphological similarity of these three blends. As shown in Fig. 3, all white spots on the fracture surfaces are MWCNTs [43]. The white spots on the cross-sections of these fibers are uniformly dispersed, indicating a relative homogeneous dispersion of MWCNTs. Owing to the small difference of polarity (γ^p) between SBS and TPU, a proper solvent cannot be found to etch one of the two phases. This has led to some difficulties in judging the localization of MWCNTs in the blends. In SBS/TPU-8NT (see the right column of Fig. 3), there are two distinct regions: one is rich in MWCNTs and the other is free of MWCNTs. Judging from the ratios of the two regions, the MWCNT-rich domains correspond to TPU, which is in good agreement with the prediction of wetting coefficient. The selective localization of MWCNTs in SBS-8NT/TPU and SBS-4NT/TPU-4NT cannot be observed very clearly under SEM. According to above mentioned thermodynamic analysis and processing methods, MWCNTs should be mainly located in SBS for SBS-8NT/TPU and both in SBS and TPU for SBS-4NT/TPU-4NT. In SBS-8NT/TPU, MWCNTs were premixed in SBS firstly for 10 min and then mixed with TPU in the second step with a much shorter period of time

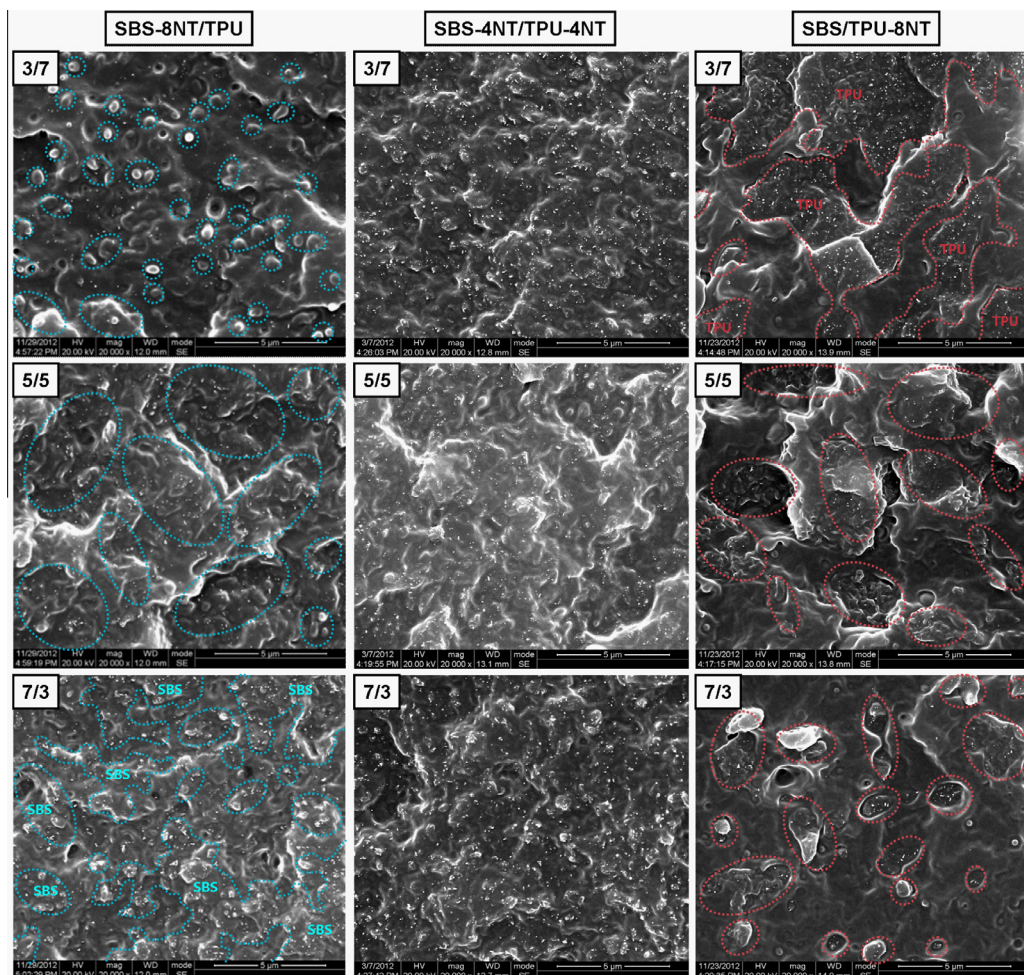


Fig. 3. SEM micrographs of the cross-sections for SBS/TPU/MWCNT composite fibers. In the green oval area, it is mainly SBS-MWCNT phase. And in the red oval area, it is mainly TPU-MWCNT phase. (For interpretation of the references to color in this figure legend, the reader is referred to the web version of this article.)

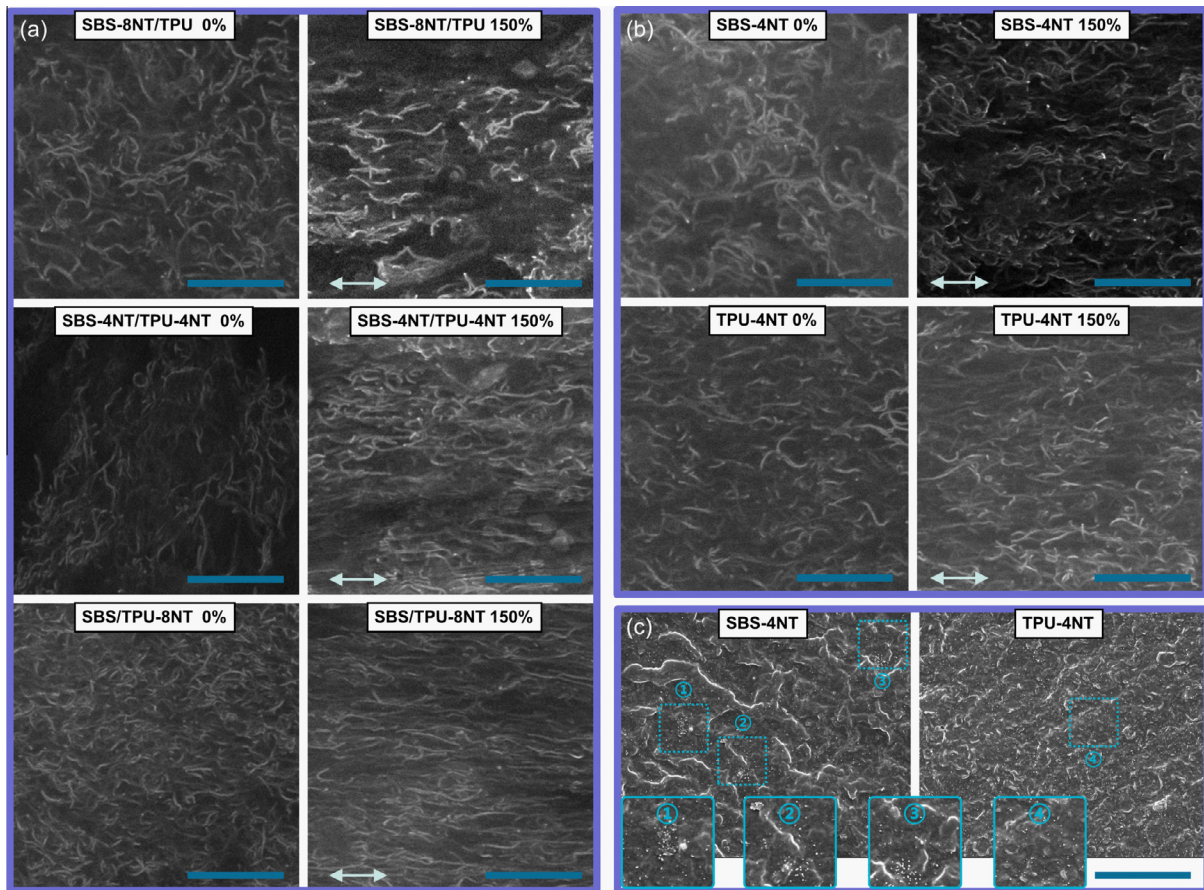


Fig. 4. SEM morphological study of composite fibers: (a) SBS/TPU/MWCNT, (b) SBS-4NT and TPU-4NT. Scale bars are 1 μm and the double arrows are along the stretching direction, and (c) SEM micrographs of the cross-sections for SBS-4NT and TPU-4NT composite fibers. Scale bars are 10 μm .

(5 min). This has minimized the possible transition of MWCNTs from SBS to TPU during the second step. Furthermore, similar polarity (γ^p) of SBS and TPU can also confirm that the possible transition between SBS and TPU is a small fraction of MWCNTs. Therefore, MWCNTs are mainly located in SBS for SBS-8NT/TPU composite (see the left column of Fig. 3). Only a small fraction of MWCNTs is located in TPU, which can be observed from the SEM image of SBS-8NT/TPU (7/3). Analogously, MWCNTs are evenly located on the fracture surfaces of SBS-4NT/TPU-4NT with different phase ratios (3/7, 5/5, 7/3), which indicates that MWCNTs are located both in SBS and TPU for SBS-4NT/TPU-4NT with direct blending of SBS-8NT and TPU-8NT in the second step (see the middle column of Fig. 3).

From above discussions, it can be noted that MWCNTs are mainly located in SBS for SBS-8NT/TPU, and in TPU for SBS/TPU-8NT. In SBS-4NT/TPU-4NT, MWCNTs are located both in SBS and TPU. Thus, the selective localization of MWCNTs might be the crucial reason for the different morphologies of initial conductive networks in the three blends, which will be further explained in the latter Section 3.3.

3.3. Morphology of conductive networks under strain: interfacial interaction

Since the electrical properties of CPCs are entirely provided by their embedded conductive networks, the morphology of conductive networks should play an important role on the strain-sensing behaviors of these CPCs. To investigate the underlying mechanism of the resistivity change under strain, the composite fibers were

observed under two different strains (0% and 150% strain) with SEM (see Fig. 4(a)) using a high accelerating voltage causing MWCNTs in the insulating polymer matrix to become charged [26]. These specimens were clamped onto sample stage under different pre-strains before observation. The bright bundles in the micrographs are MWCNTs and the grey area is polymer matrix. In the left column of Fig. 4(a), as-prepared samples show similar isotropic structure of MWCNTs. In these blends, MWCNT bundles are entangled with each other and densely dispersed in the matrix. It can be also observed that different conductive network morphologies have been constructed initially from the selective localization of MWCNTs. Owing to lower interfacial tension between TPU and MWCNT, the best dispersion quality with the densest MWCNT networks in SBS/TPU-8NT is obtained easily under the same processing conditions, which could be responsible for the highest conductivity and lowest ρ - ϵ sensitivity.

As shown in the right column of Fig. 4(a), MWCNT bundles are oriented along the stretching direction while these fibers were under 150% strain. This often leads to increased tunneling distance between local conductive networks [19]. In SBS-8NT/TPU, MWCNT bundles are relatively more distantly isolated. However, a smaller deformation of conductive networks in SBS/TPU-8NT is observed as evidenced by the dense structure of MWCNT networks. It can be also noticed that the deformation of conductive networks in SBS-4NT/TPU-4NT falls in between the two samples. Such morphology might be responsible for the higher ρ - ϵ sensitivity in SBS-8NT/TPU than SBS-4NT/TPU-4NT and SBS/TPU-8NT. The morphology of conductive networks in SBS-4NT and TPU-4NT is also investigated and shown in Fig. 4(b). In SBS-4NT and TPU-4NT

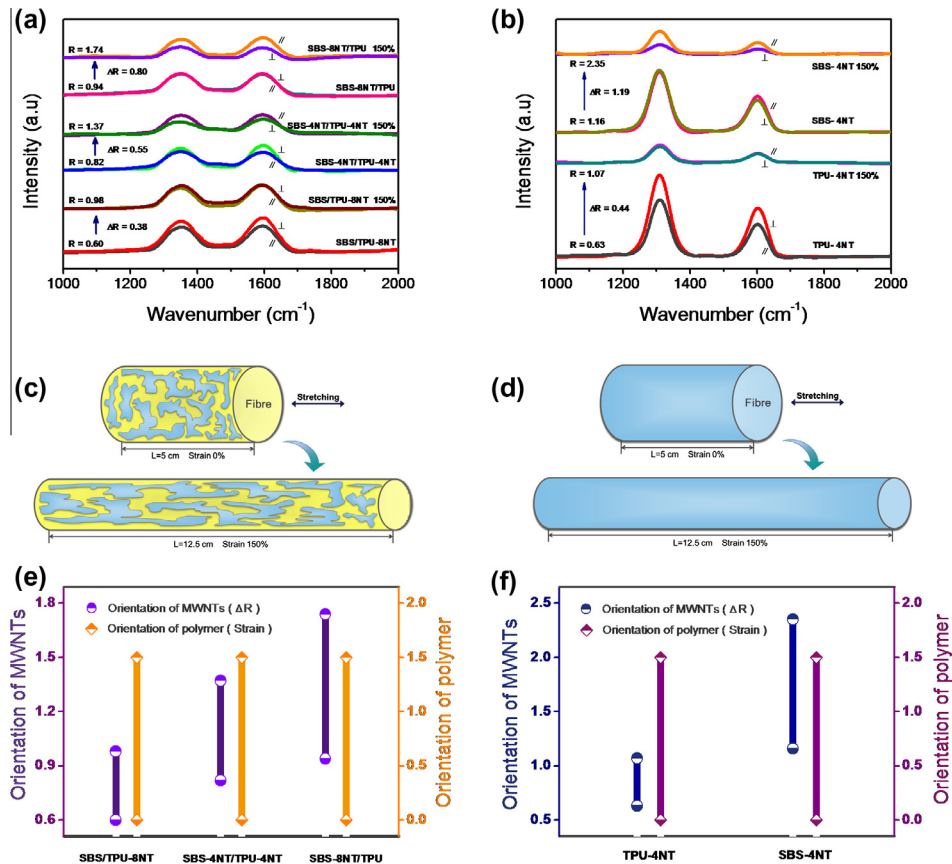


Fig. 5. Orientation measurements for SBS/TPU/MWCNT, SBS-4NT and TPU-4NT composite fibers: (a and b) Raman spectra (\parallel : parallel to stretching direction; \perp : perpendicular to stretching direction). Characteristic peaks of MWCNTs, 1580 cm^{-1} (G-band). (c and d) Sketch of composite fibers under stretching with strain from 0% to 150%. (e and f) Orientation comparison between MWCNTs and polymer.

under 0% strain, MWCNT bundles are entangled with each other. Due to the lower interfacial tension between TPU and MWCNT ($\gamma_{\text{TPU-CNT}} < \gamma_{\text{SBS-CNT}}$, see Table 2), there is a better dispersion quality in TPU-4NT as evidenced by the denser conductive network morphology comparing with SBS-4NT. Besides, the better dispersion quality can be observed in the SEM micrographs of cross-sections for SBS-4NT and TPU-4NT freeze-fractured samples (see Fig. 4(c)). In the SEM micrographs of SBS-4NT, MWCNT aggregates are obvious while hardly any MWCNT aggregate is observed in TPU-4NT. As shown in the right micrographs of Fig. 4(b), after these fibers were stretched to 150% strain, the network structures in the samples are oriented. In SBS-4NT, MWCNT bundles are relatively more distantly isolated, resulting in higher ρ - ε sensitivity. However, a smaller deformation of conductive networks is observed in TPU-4NT as evidenced by dense orientation structure of MWCNTs. Furthermore, it can be seen that MWCNT orientation in SBS-4NT is slightly more pronounced than that in TPU-4NT.

To confirm the morphology observed above, polarized Raman spectroscopy was used to quantify the orientation degree of MWCNTs (see Fig. 5(a) and (b)). Resonance-enhanced Raman scattering effect can be observed in MWCNTs while a visible or near infrared laser is used as the excitation source and such a resonance effect is not observed for polymer matrix [42]. Therefore, Raman spectroscopy is an ideal method to characterize the orientation of MWCNTs. The two bands at around 1580 cm^{-1} and 1350 cm^{-1} in the spectra are assigned to E_{2g} and A_{1g} modes, respectively. The former is denoted as the G-band generated by stretching mode of sp^2 atom pair in carbon ring or long chain and the latter is denoted as the D-band induced by structure disorder and flaw. For these CPC fibers, the Raman spectra were recorded both

parallel (\parallel) and perpendicular (\perp) the stretching direction. To evaluate the orientation degree of MWCNTs, the depolarization factor (R) was adopted, which is defined as the ratio of peak intensity for G band in the parallel direction (I_{\parallel}) to that in the perpendicular direction (I_{\perp}), I_{\parallel}/I_{\perp} . An R value close to unity indicates an isotropic morphology, whereas a value higher than unity implies preferential orientation along the stretching direction. Thus, difference of R values between unity and stretching ($\Delta R = R_{150\%} - R_{0\%}$) can be used to quantify the orientation degree of MWCNTs. Higher orientation degree contributes to larger ΔR value.

At 150% strain, SBS-4NT/TPU-4NT ($\Delta R = 0.55$) exhibits a higher ΔR value than SBS/TPU-8NT ($\Delta R = 0.38$) while SBS-8NT/TPU possesses the highest ΔR value of 0.80. Therefore, the highest orientation degree of MWCNTs in SBS-8NT/TPU is obtained among these samples, which is agrees with the above phenomenon.

The deformation of conductive networks is mainly caused by the stress transfer from polymer matrix to conductive fillers. Because of the morphological similarity in phase structure of the three blends, the strain can be simply used to evaluate the structural change of polymer matrix during stretching. Thus, the deformation of polymer matrix during stretching is studied via sustaining the same strain. The sketch of composite fiber under stretching with strain from 0% to 150% is shown in Fig. 5(c). It can be concluded that polymer matrix in the three kinds of composites respond to 150% strain in similar fashion, showing similar orientation degree around 1.5. For these three samples, the phase ratios of SBS/TPU are all 5/5 and their phase structures are almost co-continuous morphologies. Therefore, polymer matrix shows a similar orientation degree under the same strain. Similar result has been reported in our previous study [21].

Comparing the orientation of MWCNTs from Raman spectra and that of polymer matrix from strain (see Fig. 5(e)), it is noted that the orientation of polymer matrix is almost in similar fashion while conductive networks exhibit different orientation degrees. It is interesting to observe that the orientation of MWCNTs increases at different amplitudes due to different interaction between different elastomers with MWCNTs. It can be also seen that the trend in the change of conductive network morphology is well consistent with ρ - ε sensitivity. Similar results are also observed for CPC fibers of SBS-4NT and TPU-4NT (as shown in Fig. 5(b), (d) and (f)), that is SBS-4NT shows higher MWCNT orientation ($\Delta R_{\text{SBS-4NT}} = 1.19$, $\Delta R_{\text{TPU-4NT}} = 0.44$) while SBS-4NT and TPU-4NT exhibit similar orientation degree of polymer (1.5). In the Raman spectra, the G-band is generated by stretching mode of sp^2 atom pair in carbon ring or long chain and the D-band is induced by structure disorder and flaw within carbon nanotubes. As shown in Fig. 5, the intensity of Raman D-band of our single-phase composites is much higher (relative to the G-band) than in the multi-phase composites. Such difference might originate from the fact that the degree of structure disorder and flaw within carbon nanotubes in the single-phase composites is higher than that in the multi-phase composites, which could be attributed to the different processing methods. In our work, the multi-phase composites were fabricated via two-step melt-blending while the single-phase composites were fabricated via one-step melt-blending. In the second step melt-blending of the multi-phase composites, some microstructure defects within nanotubes might have been healed under the effect of shear and thermal energy, resulting in the decreasing of D-band intensity and increasing of G-band intensity. As annealing has been reported to be able to help recover the defects in CNTs [43,44].

To investigate the underlying mechanism for the different deformation behaviors of conductive networks observed above, interfacial interaction between elastomer and MWCNTs should be further studied due to its crucial role. The magnitude of the adhesion between elastomer and MWCNTs in the composites can be characterized by the thermodynamic work of adhesion (W_{AB}), which is calculated using the following formula:

$$W_{AB} = 2(\gamma_A^d \gamma_B^d)^{1/2} + 2(\gamma_A^p \gamma_B^p)^{1/2} \quad (4)$$

where W_{AB} is the work of adhesion between components A and B. The W_{AB} values of SBS-MWCNT and TPU-MWCNT are 73.2 mN/m and 67.7 mN/m, respectively. The higher value of W_{AB} indicates stronger interaction between two components, thus such interface will be relatively stronger. W_{AB} of SBS-MWCNT is higher than that of TPU-MWCNT, which indicates good adhesion between SBS and MWCNTs. This strong interaction between SBS and MWCNTs has also been reported elsewhere [45]. It is caused by the π - π conjunction between the aromatic structure of SBS, the double bonds in SBS chains and MWCNTs. Therefore, strong interfacial interaction realizes efficient load transfer from SBS to MWCNTs. As a result, conductive networks are easily deformed under strain. On the other hand, the interaction between TPU and MWCNTs is relatively weaker than SBS-MWCNT, which induces less efficient stress transfer, lower orientation of MWCNTs (see Fig. 5(b) and (f)) and thus lower ρ - ε sensitivity.

Besides above mentioned issues, with smaller differences in surface energy and polarity of TPU and MWCNTs, the best dispersion quality with the densest MWCNT networks in SBS/TPU-8NT may be achieved. This might result in smaller deformation of conductive networks compared to SBS-8NT/TPU and SBS-4NT/TPU-4NT. Meanwhile, owing to the poorer dispersion, MWCNT bundles in SBS are relatively more distantly isolated under strain. Therefore, the conductive networks are easily destructed in SBS-8NT/TPU which leads to the highest ρ - ε sensitivity.

3.4. Modeling and mechanism

To understand the mechanism of resistivity-strain sensing behavior further, modeling study is carried out. According to the model derived from tunneling theory by Simmons [46], the total resistance R of the CPCs can be represented by Eq. (5).

$$R = \left(\frac{L}{N}\right) \left(\frac{8\pi h s}{3\gamma a^2 e^2}\right) \exp(\gamma s) \quad (5)$$

$$\gamma = 4\pi\sqrt{2m\phi}/h$$

where L is the number of particles forming a single conductive pathway, N is the number of conductive pathways, h is the Planck's constant, s is the least distance between conductive particles, a^2 is the effective cross-section area, e is the electron charge, m is the electron mass and ϕ is the height of potential barrier between adjacent particles.

While strain is applied to the composites, resistance will be altered due to particle separation and the inter-particle distance changes linearly and proportionally with increased strain from s_0 to s . Then, it can be expressed as follows:

$$s = s_0(1 + C\varepsilon) = s_0 \left[1 + C\left(\frac{\Delta l}{l_0}\right)\right] \quad (6)$$

where ε is the tensile strain of the composites, Δl is the deformation of the composite samples, and l_0 is the initial length of the samples.

Due to the high rate of resistivity increase at larger strain, it is assumed that the number of conductive pathways changes at a much higher rate, and can be expressed as follows [47]:

$$N = \frac{N_0}{\exp(M\varepsilon + W\varepsilon^2 + U\varepsilon^3 + V\varepsilon^4)} \quad (7)$$

where M , W , U and V are constants.

The substitution of Eqs. (6) and (7) into Eq. (5) yields Eq. (8):

$$R = \frac{8\pi n h s_0}{2\gamma N_0^2 a^2 e^2} (1 + C\varepsilon) \exp[\gamma s + (2M + \gamma s C)\varepsilon + 2W\varepsilon^2 + 2U\varepsilon^2 + 2V\varepsilon^2] \\ = B(1 + C\varepsilon) \exp[A + (2M + AC)\varepsilon + 2W\varepsilon^2 + 2U\varepsilon^2 + 2V\varepsilon^2] \quad (8)$$

$$A = \gamma s$$

$$B = \frac{8\pi n h s_0}{2\gamma N_0^2 a^2 e^2}$$

It is shown in Fig. 6(a) that the model of tunneling currents describes the experimental data quite well. Fitting parameters are listed in Table 3. The calculated change of conductive pathways (change of CP, $M\varepsilon + W\varepsilon^2 + U\varepsilon^3 + V\varepsilon^4$) and change of tunneling distance (change of TD, $C\varepsilon$) are plotted against strain as shown in Fig. 6(b) and (c), respectively. It is observed that the number of conductive pathways in SBS-8NT/TPU decreases much faster than that in SBS-4NT/TPU-4NT and SBS/TPU-8NT, indicating that the conductive networks of SBS-8NT/TPU deform more greatly under strain than those of SBS-4NT/TPU-4NT and SBS/TPU-8NT. Besides, the tunneling distance of MWCNTs in SBS-8NT/TPU increases at a higher rate than those in SBS-4NT/TPU-4NT and SBS/TPU-8NT. The two aspects are in agreement with above experimental results.

To describe the resistivity-strain sensing behavior of different CPC blends and illustrate the responsible mechanism, sketch is drawn according to the above discussion. As shown in Fig. 7(a) and (b), the change of conductive networks and phase continuity under strain is illustrated. Both MWCNTs and polymer matrix are oriented under strain. With the co-continuous phase morphology in the three samples, a similar orientation degree of polymer

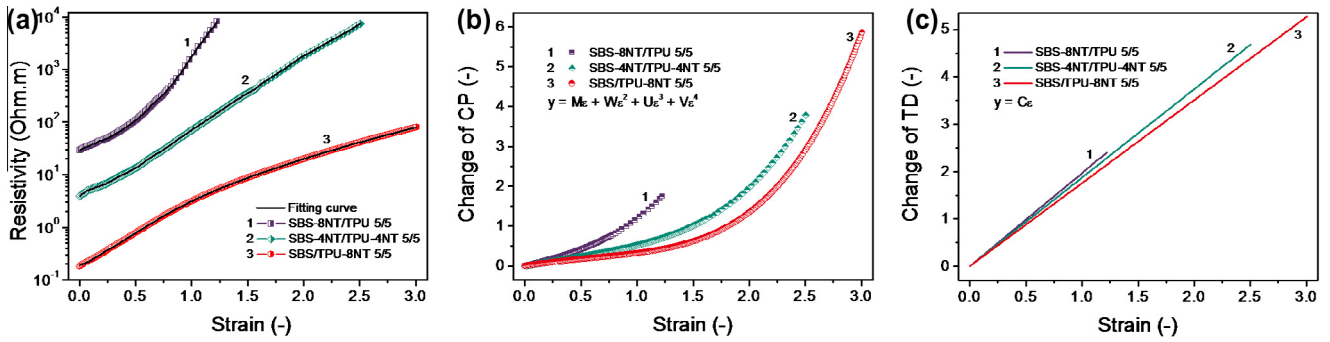


Fig. 6. (a) Experimental (dots), theoretical (black solid lines) data of strain-dependent resistivity. Change of (b) conductive pathways and (c) tunneling distance as a function of strain.

Table 3

Parameters obtained by fitting the data with Eq. (8).

	A	B	C	M	W	U	V	AC+2M
SBS/TPU-8NT	0.64	0.10	1.75	0.41	-0.15	-0.02	0.08	1.94
SBS-4NT/TPU-4NT	1.10	0.45	1.87	0.49	-0.03	-0.01	0.07	3.04
SBS-8NT/TPU	1.27	1.31	1.97	0.65	0.24	0.16	0.14	3.80

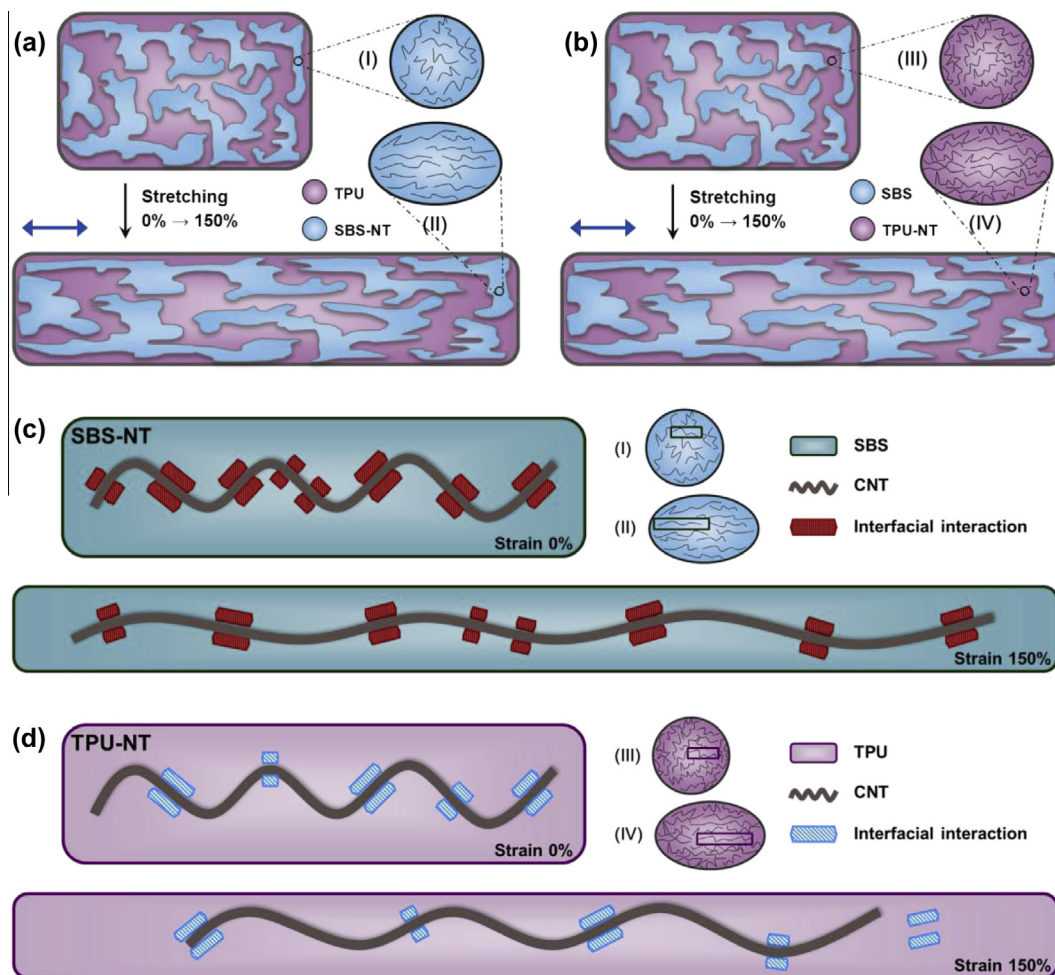


Fig. 7. Sketch of conductive network and phase continuity change during stretching for composite fibers with 2 different localizations of MWCNTs.

matrix is achieved in these CPCs (see Fig. 5(e)). Moreover, with the same overall MWCNT content in these blends, the effect of MWCNT content can be isolated. Thus, the different orientation degree of MWCNTs should be attributed to different interactions

between polymer matrix and MWCNTs. A larger interaction often leads to higher orientation degree. For SBS-8NT/TPU, MWCNTs are mainly located in SBS (see Fig. 7(a)). The presence of double bonds and aromatic rings in the SBS chains are expected to

enhance the interaction between polymer and MWCNTs [49]. Therefore, strong interfacial interaction realizes efficient load transfer from SBS to MWCNTs when SBS-8NT/TPU is stretched. As a result, the conductive networks are easily deformed with increasing strain (see Fig. 7(c)). On the other hand, MWCNTs are located in TPU for SBS/TPU-8NT (see Fig. 7(b)). The interaction between TPU and MWCNT is relative weaker than SBS–MWCNT in spite of high polarity of polyurethane chains, which induces less efficient stress transfer, smaller orientation of MWCNTs and thus lower ρ - ε sensitivity (see Fig. 7(d)). As shown in Fig. 7(c) and (d), the conclusion can be drawn as that there are much more “connections of interfacial interaction” between SBS and MWCNT than TPU–MWCNT. In addition, these connections can limit the slippage between polymer matrix and filler with more efficient stress transfer. Therefore, strong interfacial interaction leads to high orientation degree of filler. In view of the above two aspects, in SBS-4NT/TPU-4NT with MWCNTs being located both in SBS and TPU, two kinds of interactions (SBS–MWCNT, TPU–MWCNT) are beneficial for the deformation of conductive networks, which result in the medial ρ - ε sensitivity.

4. Conclusions

In conclusion, it has been demonstrated that it is possible to fabricate SBS/TPU/MWCNT composite fibers with selective localization of MWCNTs in the blends via three different melt processing procedures. MWCNTs are mainly located in SBS for SBS-8NT/TPU, and in TPU for SBS/TPU-8NT. In SBS-4NT/TPU-4NT, MWCNTs are located both in SBS and TPU. Thus, different conductive network morphologies and interfacial interactions between elastomer and MWCNTs were constructed, resulting in different resistivity–strain sensitivities. Through a series of characterization methods, including SEM, Polarized Raman spectra etc., it is observed that high orientation of MWCNTs is pronounced while these fillers are located in SBS. To understand the MWCNT dispersion and interfacial interaction for TPU–MWCNT and SBS–MWCNT, wetting coefficient calculation and thermodynamic work of adhesion calculation have been carried out. Wetting coefficient calculation suggests that slightly better wetting of MWCNTs with TPU, however, work of adhesion calculation indicates the presence of stronger interfacial interaction between MWCNTs and SBS. Such strong interfacial interaction is thought as crucial for the enhanced resistivity–strain sensitivity. Furthermore, the relative poorer dispersion of MWCNTs in SBS is thought as another possible responsible issue due to the slightly poorer wetting between SBS and MWCNTs. This study indicates that the resistivity–strain sensitivity can be tuned by using polymer blends with different localizations of fillers. Furthermore, it was observed that the change in tunneling distance and the number of conductive pathways could be accelerated significantly with enhanced interfacial interaction. This study provides a new and simple route for the fabrication of CPCs with tunable resistivity–strain sensitivity.

Acknowledgements

We express our sincere thanks to the National Natural Science Foundation of China for financial support (51003063, 51273117 and 51121001). This work was subsidized by the special funds for Major State Basic Research Projects of China (2011CB606006).

References

- [1] Dai K, Xu X-B, Li Z-M. Electrically conductive carbon black (CB) filled in situ microfibrillar poly(ethylene terephthalate) (PET)/polyethylene (PE) composite with a selective CB distribution. *Polymer* 2007;48(3):849–59.
- [2] Li C, Thostenson ET, Chou T-W. Sensors and actuators based on carbon nanotubes and their composites: a review. *Compos Sci Technol* 2008;68(6):1227–49.
- [3] Pham GT, Park Y-B, Liang Z, Zhang C, Wang B. Processing and modeling of conductive thermoplastic/carbon nanotube films for strain sensing. *Composites Part B-Eng* 2008;39(1):209–16.
- [4] Gao L, Chou T-W, Thostenson ET, Zhang Z, Coulaud M. In situ sensing of impact damage in epoxy/glass fiber composites using percolating carbon nanotube networks. *Carbon* 2011;49(10):3382–5.
- [5] Lim AS, Melrose ZR, Thostenson ET, Chou T-W. Damage sensing of adhesively-bonded hybrid composite/steel joints using carbon nanotubes. *Compos Sci Technol* 2011;71(9):1183–9.
- [6] Abraham JK, Philip B, Wittchurch A, Varadan VK, Reddy CC. A compact wireless gas sensor using a carbon nanotube/PMMA thin film chemiresistor. *Smart Mater Struct* 2004;13(5):1045–9.
- [7] Valentini L, Armentano I, Kenny JM, Cantalini C, Lozzi L, Santucci S. Sensors for sub-ppm NO₂ gas detection based on carbon nanotube thin films. *Appl Phys Lett* 2003;82(6):961–3.
- [8] Kobashi K, Villmow T, Andres T, Poetschke P. Liquid sensing of melt-processed poly(lactic acid)/multi-walled carbon nanotube composite films. *Sens Actuators, B-Chem* 2008;134(2):787–95.
- [9] Poetschke P, Andres T, Villmow T, Pegel S, Bruenig H, Kobashi K, et al. Liquid sensing properties of fibres prepared by melt spinning from poly(lactic acid) containing multi-walled carbon nanotubes. *Compos Sci Technol* 2010;70(2):343–9.
- [10] Villmow T, John A, Poetschke P, Heinrich G. Polymer/carbon nanotube composites for liquid sensing: selectivity against different solvents. *Polymer* 2012;53(14):2908–18.
- [11] An KH, Jeong SY, Hwang HR, Lee YH. Enhanced sensitivity of a gas sensor incorporating single-walled carbon nanotube-polyppyrrrole nanocomposites. *Adv Mater* 2004;16(12):1005–9.
- [12] Castro M, Lu J, Bruzaud S, Kumar B, Feller J-F. Carbon nanotubes/poly(epsilon-caprolactone) composite vapour sensors. *Carbon* 2009;47(8):1930–42.
- [13] Lu J, Kumar B, Castro M, Feller J-F. Vapour sensing with conductive polymer nanocomposites (CPC): polycarbonate-carbon nanotubes transducers with hierarchical structure processed by spray layer by layer. *Sens Actuators, B-Chem* 2009;140(2):451–60.
- [14] Ferrer-Anglada N, Kaempgen M, Roth S. Transparent and flexible carbon nanotube/polyppyrrrole and carbon nanotube/polyaniline pH sensors. *Phys Status Solidi B-Basic Solid State Phys* 2006;243(13):3519–23.
- [15] Bilotti E, Zhang R, Deng H, Baxendale M, Peijs T. Fabrication and property prediction of conductive and strain sensing TPU/CNT nanocomposite fibres. *J Mater Chem* 2010;20(42):9449–55.
- [16] de la Vega A, Kinloch IA, Young RJ, Bauhofer W, Schulte K. Simultaneous global and local strain sensing in SWCNT-epoxy composites by Raman and impedance spectroscopy. *Compos Sci Technol* 2011;71(2):160–6.
- [17] Lin L, Deng H, Gao X, Zhang S, Bilotti E, Peijs T, et al. Modified resistivity–strain behavior through the incorporation of metallic particles in conductive polymer composite fibers containing carbon nanotubes. *Polym Int* 2013;62(1):134–40.
- [18] Dang Z-M, Jiang M-J, Xie D, Yao S-H, Zhang L-Q, Bai J. Supersensitive linear piezoresistive property in carbon nanotubes/silicone rubber nanocomposites. *J Appl Phys* 2008;104(2).
- [19] Murugaraj P, Mainwaring D, Khelil NA, Peng JL, Siegle R, Sawant P. The improved electromechanical sensitivity of polymer thin films containing carbon clusters produced in situ by irradiation with metal ions. *Carbon* 2010;48(15):4230–7.
- [20] Hwang J, Jang J, Hong K, Kim KN, Han JH, Shin K, et al. Poly(3-hexylthiophene) wrapped carbon nanotube/poly(dimethylsiloxane) composites for use in finger-sensing piezoresistive pressure sensors. *Carbon* 2011;49(1):106–10.
- [21] Lin L, Liu S, Zhang Q, Li X, Ji M, Deng H, et al. Towards tunable sensitivity of electrical property to strain for conductive polymer composites based on thermoplastic elastomer. *ACS Appl Mater Interfaces* 2013;5(12):5815–24.
- [22] Pang H, Yan D-X, Bao Y, Chen J-B, Chen C, Li Z-M. Super-tough conducting carbon nanotube/ultra-high-molecular-weight polyethylene composites with segregated and double-percolated structure. *J Mater Chem* 2012;22(44):23568–75.
- [23] Su C, Xu L, Zhang C, Zhu J. Selective location and conductive network formation of multiwalled carbon nanotubes in polycarbonate/poly(vinylidene fluoride) blends. *Compos Sci Technol* 2011;71(7):1016–21.
- [24] Gao J-F, Yan D-X, Yuan B, Huang H-D, Li Z-M. Large-scale fabrication and electrical properties of an anisotropic conductive polymer composite utilizing preferable location of carbon nanotubes in a polymer blend. *Compos Sci Technol* 2010;70(13):1973–9.
- [25] Chen L, Zhang XL, Li HY, Li B, Wang K, Zhang Q, et al. Superior tensile extensibility of PETG/PC amorphous blends induced via uniaxial stretching. *Chin J Polym Sci* 2011;29(1):125–32.
- [26] Kovacs JZ, Andresen K, Pauls JR, Garcia CP, Schossig M, Schulte K, et al. Analyzing the quality of carbon nanotube dispersions in polymers using scanning electron microscopy. *Carbon* 2007;45(6):1279–88.
- [27] Zhang R, Dowden A, Deng H, Baxendale M, Peijs T. Conductive network formation in the melt of carbon nanotube/thermoplastic polyurethane composite. *Compos Sci Technol* 2009;69(10):1499–504.
- [28] Chen L, Chen G, Lu L. Piezoresistive behavior study on finger-sensing silicone rubber/graphite nanosheet nanocomposites. *Adv Funct Mater* 2007;17(6):898–904.

- [29] Flandin L, Brechet Y, Cavaille JY. Electrically conductive polymer nanocomposites as deformation sensors. *Compos Sci Technol* 2001;61(6): 895–901.
- [30] Chen J, Du X-C, Zhang W-B, Yang J-H, Zhang N, Huang T, et al. Synergistic effect of carbon nanotubes and carbon black on electrical conductivity of PA6/ABS blend. *Compos Sci Technol* 2013;81:1–8.
- [31] Yan D, Li X, Ma H-L, Tang X-Z, Zhang Z, Yu Z-Z. Effect of compounding sequence on localization of carbon nanotubes and electrical properties of ternary nanocomposites. *Composites Part A-Appl Sci Manuf* 2013;49: 35–41.
- [32] Bose S, Bhattacharyya AR, Kulkarni AR, Poetschke P. Electrical, rheological and morphological studies in co-continuous blends of polyamide 6 and acrylonitrile-butadiene-styrene with multiwall carbon nanotubes prepared by melt blending. *Compos Sci Technol* 2009;69(3–4):365–72.
- [33] Goeldel A, Kasaliwal G, Poetschke P. Selective localization and migration of multiwalled carbon nanotubes in blends of polycarbonate and poly(styrene-acrylonitrile). *Macromol Rapid Commun* 2009;30(6):423–9.
- [34] Shi Y, Li Y, Wu J, Huang T, Chen C, Peng Y, et al. Toughening of poly(l-lactide)/ multiwalled carbon nanotubes nanocomposite with ethylene-co-vinyl acetate. *J Polym Sci Part B-Polym Phys* 2011;49(4):267–76.
- [35] Wu D, Lin D, Zhang J, Zhou W, Zhang M, Zhang Y, et al. Selective localization of nanofillers: effect on morphology and crystallization of PLA/PCL blends. *Macromol Chem Phys* 2011;212(6):613–26.
- [36] Wu DF, Zhang YS, Zhang M, Yu W. Selective localization of multiwalled carbon nanotubes in poly(epsilon-caprolactone)/polylactide blend. *Biomacromolecules* 2009;10(2):417–24.
- [37] Wu M, Shaw LL. On the improved properties of injection-molded, carbon nanotube-filled PET/PVDF blends. *J Power Sources* 2004;136(1):37–44.
- [38] Souheng W. *Polymer interface and Adhesion*. New York: Marcel Dekker Inc.; 1982.
- [39] Baudouin A-C, Devaux J, Bailly C. Localization of carbon nanotubes at the interface in blends of polyamide and ethylene-acrylate copolymer. *Polymer* 2010;51(6):1341–54.
- [40] Fenouillot F, Cassagnau P, Majeste JC. Uneven distribution of nanoparticles in immiscible fluids: morphology development in polymer blends. *Polymer* 2009;50(6):1333–50.
- [41] Lu L, Zhou Z, Zhang Y, Wang S, Zhang Y. Reinforcement of styrene-butadiene-styrene tri-block copolymer by multi-walled carbon nanotubes via melt mixing. *Carbon* 2007;45(13):2621–7.
- [42] Bhattacharyya AR, Sreekumar TV, Liu T, Kumar S, Ericson LM, Hauge RH, et al. Crystallization and orientation studies in polypropylene/single wall carbon nanotube composite. *Polymer* 2003;44(8):2373–7.
- [43] Ni ZH, Wang YY, Yu T, Shen ZX. Raman spectroscopy and imaging of graphene. *Nano Res* 2008;1(4):273–91.
- [44] Kim YA, Hayashi T, Osawa K, Dresselhaus MS, Endo M. Annealing effect on disordered multi-wall carbon nanotubes. *Chem Phys Lett* 2003;380(3–4):319–24.
- [45] Inukai S, Niihara K-i, Noguchi T, Ueki H, Magario A, Yamada E, et al. Preparation and properties of multiwall carbon nanotubes/polystyrene-block-polybutadiene-block-polystyrene composites. *Ind Eng Chem Res* 2011;50(13):8016–22.
- [46] Simmons JG. *Journal of Applied Physics* 1963;34(6):1793–803.
- [47] Ping S, Sichel EK, Gittleman JI. Fluctuation-induced tunneling conduction in carbon-polyvinylchloride composites. *Phys Rev Lett* 1978;40(18):1197–200.
- [48] Barber AH, Cohen SR, Wagner HD. Static and dynamic wetting measurements of single carbon nanotubes. *Phys Rev Lett* 2004;92(18).
- [49] Pedroni LG, Soto-Oviedo MA, Rosolen JM, Felisberti MI, Nogueira AF. Conductivity and mechanical properties of composites based on MWCNTs and styrene-butadiene-styrene block (TM) copolymers. *J Appl Polym Sci* 2009;112(6):3241–8.